Evolution of hydrogen dissolution and superconductivity in Re-based solid solutions under pressure studied by *ab initio* calculations

Shuhan Yang,[1,*] Quan Zhuang,[2,*] Xilian Jin,[1,†] Liying Song,[1] Li Zhang,[1] Tian Cui,[1,3] and Bingbing Liu[1]

[1]*State Key Laboratory of Superhard Materials, College of Physics, Jilin University, Changchun 130012, China*

[2]*Inner Mongolia Key Laboratory of Carbon Nanomaterials, Nano Innovation Institute (NII), College of Chemistry and Materials Science, Inner Mongolia University for Nationalities, Tongliao 028000, China*

[3]*School of Physical Science and Technology, Ningbo University, Ningbo 315211, China*

(Received 26 November 2020; revised 10 May 2021; accepted 11 May 2021; published 28 May 2021)

The dissolving of hydrogen (H) into rhenium (Re) is non-negligible in high-pressure experiments involving dense hydrogen and hydrogenous materials, in which rhenium is often used as a gasket material in the high-pressure diamond-anvil cell devices. However, the evolution of hydrogen dissolution into Re and the pressure-induced effects of hydrogen coupling on the superconductivity of metal-based hydrides remain poorly understood experimentally, and theoretical investigations are currently lacking. The present work addresses these issues by applying *ab initio* calculations for systematically investigating the dissolution of H atoms in Re systems, as well as the electronic properties, lattice dynamics, and electron-phonon coupling (EPC) in the corresponding interstitial Re hydrides. A series of ReH_x compounds with increasing x in the range of 0 to 1 in increments of 0.125 are predicted to be stable at increasing pressures ranging from 1 to 50 GPa. It is found that H atoms generally play the role of impurities in the ReH_x compounds except for $ReH_{0.5}$ and ReH, where H atoms are integrated into the crystal structure. Moreover, the atomic configuration of the Re host lattice is basically preserved with increasing x and increasing pressure. Further analysis of the superconductive mechanism indicates that an increasing H concentration results in a decreased electronic density of states at the Fermi level and increasing phonon frequencies, which lead to a decrease of EPC λ and superconducting critical temperature. These findings quantitatively clarify the effects of hydrogen doping on superconductivity in metal-based hydrides, and thereby support the exploration of new types of superconductive hydrides.

DOI: 10.1103/PhysRevB.103.174520

I. INTRODUCTION

High-pressure conditions have been demonstrated to enable the production of materials with unusual properties that cannot be fabricated under an ambient pressure condition [1–9]. One of the many attractive applications of high-pressure fabrication involves the development of superconducting materials arising from the metallization of solid hydrogen that has been reported to occur under high-pressure conditions [10–13]. In addition, the work of Ashcroft in 2004 [14] has demonstrated an ability to obtain hydrogen-dominant metallic alloys with superconducting properties at much lower pressures than required for pure solid hydrogen. This has led to the extensive investigation of hydrogen-rich compounds for seeking the superconductors with high superconducting critical temperature (T_c) values and clarifying the high-T_c mechanism of superconductivity [3–5,15,16].

The above-discussed experimental work relies heavily on high-pressure diamond-anvil cell (DAC) devices composed of two diamond heads between which a small sample is placed [12,17–19]. However, the solid hydrogen or metallic hydride samples employed in these experiments may decompose and release hydrogen atoms. Therefore, DAC devices generally employ a thin foil composed of a strong metal, such as rhenium (Re), platinum (Pt), or tungsten (W), as a gasket inserted between the two diamond heads of the DAC apparatus. While this precaution does contain the sample, the hydrogen released during sample decomposition can diffuse into the diamond anvils and metal gasket, and cause hydrogen embrittlement. Here, the hydrogen embrittlement of the diamond anvils results in a cracking phenomenon that is readily apparent. In contrast, the diffusion of hydrogen into the interstitial lattice sites of the metal gasket can occur without being noticed, which can lead to very puzzling measurement results [17]. Accordingly, the negative influence of hydrogen diffusion into the gasket material employed in high-pressure experimental equipment cannot be neglected during high-pressure experiments.

The high bulk modulus of 370 GPa and low brittleness of Re makes this the standard gasket material employed in high-pressure experiments [20,21]. Moreover, this gasket material has been adopted in numerous studies involving high-T_c superconducting materials such as solid hydrogen, hydrogen-rich compounds, and superhydrides [22–25]. Nonetheless, hydrogen diffusion into Re gasket materials has not been thoroughly explored [26]. At room temperature, the hydrogenation process in Re has been demonstrated to initiate at a pressure of 5.3 GPa, and an early saturation was shown to

*These authors contributed equally to this work

†jinxilian@jlu.edu.cn

occur with the formation of $ReH_{0.38}$ at a pressure of 8.6 GPa, indicating a hydrogen solubility of approximately 0.38 [27]. Subsequently, Besedin and Jephcoat [28] proposed that the hydrogen solubility of Re was approximately 0.38 up to a pressure of 120 GPa at room temperature. Kawamura *et al.* [29] reported that $ReH_{0.36}$ formed a layered structure at room temperature, where hydrogen atoms occupied only every second layer along the *c* axis in the hexagonal close-packed (hcp) lattice of Re, resulting in an anti-CdI_2 type structure. Scheler *et al.* [21] later reported that the room-temperature hydrogen solubility of Re hydrides with a layered anti-CdI_2 type structure was observed to increase to approximately 0.5 over time at a pressure of 15 GPa. Moreover, they expanded the temperature range of DAC experiments to a temperature of 420 K, and demonstrated the stable high-temperature formation of $ReH_{0.85}$ hydrides with a NiAs-type structure at a pressure of 23 GPa. Finally, the possibility of forming fully stoichiometric Re hydride (ReH) at high temperatures and pressures greater than 50 GPa was discussed.

In addition to the above-discussed surveys of hydrogen diffusion in Re, a few studies have investigated the superconductivity of H-doped Re solid solutions at high pressure experimentally. For example, Antonov *et al.* [30] explored the hydrogen-concentration dependence of T_c in Re-H solid solutions at pressures of up to 9 GPa. The hydrogen solubility in Re was found to increase monotonically with increasing pressure with a maximum of approximately 0.23 obtained at a pressure of 9 GPa, while T_c decreased with further increase in the pressure. Interestingly, the T_c value returned to the values observed for the original Re metal after the removal of hydrogen from the Re-H samples via vacuum annealing at 773 K, which clearly demonstrated the relationship between T_c and the hydrogen concentration in Re-H solid solutions.

The studies discussed above demonstrate the difficulty of establishing a comprehensive experimental basis for evaluating the evolution of hydrogen dissolution in Re, and particularly for understanding the pressure-induced effects of hydrogen coupling on the superconductivity of metal-based hydrides. Clearly, a theoretical basis is required. However, these issues have not yet been subjected to theoretical investigation.

The present study addresses this issue by systematically investigating the dissolution of hydrogen in Re, as well as the electronic properties, lattice dynamics, and electron-phonon coupling (EPC) in the corresponding interstitial hydrides by *ab initio* calculations. A series of hydrogen-doped Re compounds (HDRCs) with increasing hydrogen concentration in the range of 0 to 1 in increments of 0.125 are predicted to be stable under pressures ranging from 1 to 50 GPa. Here, the hydrogen solubility is found to increase monotonically with pressurization, and the fully stoichiometric ReH compound is predicted to form at 35 GPa. The effects of hydrogen concentration on the EPC of the HDRCs are further analyzed by comparing the pressure dependence of the EPC parameter λ in pure Re and HDRC systems. The extent of electron donation from the Re atoms increases with increasing hydrogen concentration, and leads to a decrease in the electronic density of states $N(\varepsilon_F)$ at the Fermi energy ε_F. Moreover, the phonon frequencies are increased with increasing hydrogen concentration due to the lower mass of the hydrogen atoms. These two factors result in a decrease in the value of λ with increasing hydrogen concentration. The findings of this study provide useful insights for understanding the high-pressure behavior of hydrogen in solid solutions and superconductivity in metal-based hydrides.

II. COMPUTATIONAL DETAILS

The HDRC structures were determined in the pressure range of 1 bar to 50 GPa using the ELocR code developed by our group [31,32] (and see Supplemental Material Refs. [33–37]). The Vienna *Ab initio* Simulation Package (VASP) [38] was employed for calculating the underlying *ab initio* structural relaxations and electronic properties based on density-functional theory using the Perdew-Burke-Ernzerhof (PBE) formulation of the generalized gradient approximation [39]. Interactions among the electrons and ions were simulated using the projector augmented-wave (PAW) method. The atomic radius of Re was set as 2.3 a.u. based on $5p6s5d$ electrons and the atomic radius of hydrogen was set as 0.8 a.u. based on $1s$ electrons. The numbers of electrons assigned as valence electrons for the H and Re atoms were 1 and 15, respectively. The convergence of the total-energy calculations was ensured by applying a plane-wave kinetic energy cutoff of 1000 eV for the pure Re and HDRC systems. Appropriate Monkhorst-Pack *k* meshes with a grid spacing of $2\pi \times 0.025$ Å^{-1} were adopted.

Phonon and electron-phonon interaction calculations of the pure Re and HDRC systems were computed using the QUANTUM-ESPRESSO code [40]. We employed PAW pseudopotentials with PBE exchange-correlation functionals for both Re and H atoms [41]. Cutoff energies of 80 and 100 Ry were, respectively, adopted for the pure Re and HDRC systems. The *q*-point meshes employed in the first Brillouin zone for phonon and electron-phonon interaction calculations were $5 \times 5 \times 3$ for the pure Re system ($P6_3/mmc$ space group), $4 \times 4 \times 4$ for the $ReH_{0.125}$ system (P-$3m1$ space group), $4 \times 6 \times 4$ for the $ReH_{0.25}$ system ($P2/m$ space group), $5 \times 5 \times 3$ for the $ReH_{0.5}$ system (P-$3m1$ space group), $4 \times 4 \times 4$ for the $ReH_{0.667}$ system (P-$3m1$ space group), $4 \times 6 \times 3$ for the $ReH_{0.75}$ system ($P2/m$ space group), and $8 \times 8 \times 5$ for the ReH system ($P6_3/mmc$ space group). Finally, the phonon spectra and phonon density of states were calculated via the linear-response method [42].

The superconductivity mechanism of HDRCs was studied within the framework of Bardeen-Cooper-Schrieffer theory. The value of T_c was evaluated based on the following Allen-Dynes modified McMillan equation [43]:

$$T_c = \frac{\omega_{\log}}{1.2}\exp\left[-\frac{1.04(1+\lambda)}{\lambda - \mu^* 1 + 0.62\lambda}\right], \tag{1}$$

where $\omega_{\log}$ is the average logarithmic value of the phonon frequency ω and μ^* is the Coulomb pseudopotential. The values of λ and $\omega_{\log}$ can be obtained by the integrals

$$\lambda = 2\int_0^\infty \frac{\alpha^2 F(\omega)}{\omega} d\omega \tag{2}$$

and

$$\omega_{\log} = \exp\left(\frac{2}{\lambda}\int_0^\infty \frac{d\omega}{\omega}\alpha^2F(\omega)\ln\omega\right), \tag{3}$$

where $\alpha^2F(\omega)$ is the Eliashberg spectral function:

$$\alpha^2F(\omega) = \frac{1}{2\pi N(\varepsilon_F)}\sum_{\mathbf{q}\upsilon}\frac{\gamma_{\mathbf{q}\upsilon}}{\omega_{\mathbf{q}\upsilon}}\delta(\omega-\omega_{\mathbf{q}\upsilon}). \tag{4}$$

Here, $\delta(\cdot)$ is the Dirac delta function, $\gamma_{\mathbf{q}\upsilon}$ is the phonon linewidth given by

$$\gamma_{\mathbf{q}\upsilon} = \pi\omega_{\mathbf{q}\upsilon}\sum_{mn}\sum_{\mathbf{k}}\left|g^{\upsilon}_{mn}(\mathbf{k},\mathbf{q})\right|^2\delta(\varepsilon_{m,\mathbf{k}+\mathbf{q}}-\varepsilon_F) \times\delta(\varepsilon_{n,\mathbf{k}}-\varepsilon_F), \tag{5}$$

and $\omega_{\mathbf{q}\upsilon}$ is the phonon frequency of the mode υ at the wave vector $\mathbf{q}$. Finally, the overall value of λ can be expressed as

$$\lambda = \sum_{\mathbf{q}\upsilon}\lambda_{\mathbf{q}\upsilon} = \sum_{\mathbf{q}\upsilon}\frac{\gamma_{\mathbf{q}\upsilon}}{\pi N(\varepsilon_F)\omega^2_{\mathbf{q}\upsilon}}. \tag{6}$$

The effect of hydrogen atoms as an impurity in HDRCs was investigated based on the previously proposed effective band structure (EBS) method [44,45]. As is well known, the EBS method enables a convenient analysis of the electronic band structure in alloys via an unfolding mechanism, and provides valuable information that can be compared with experimental measurements (e.g., angle-resolved photoemission spectroscopy measurements). The unfolded electronic band structures can be plotted based on the information of the spectral function. The spectral function of continuous eigenvalue variable E can be calculated according to the eigenvalues and eigenfunctions of a supercell (SC), which can be described as follows [46]:

$$A(\vec{k},E) = \sum_m P_{\vec{K}m}(\vec{k})\delta(E_{\vec{K}m}-E). \tag{7}$$

Here, $\vec{k}$ and $\vec{K}$, respectively, denote the wave vectors corresponding to the primitive cell (PC) and the reciprocal space of the SC, m is the band index pertaining to $\vec{K}$, and $P_{\vec{K}m}$ represents the spectral weight, which can be defined as

$$P_{\vec{K}m}(\vec{k}) = \sum_n |\langle\vec{K}m|\vec{k}n\rangle|^2, \tag{8}$$

where n is the band index pertaining to $\vec{k}$. Obviously, $P_{\vec{K}m}$ represents information regarding the extent to which the characteristics of the PC state $|\vec{k}n\rangle$ are preserved in the SC state $|\vec{K}m\rangle$. In the case of the SC, the spectral weight satisfies the equation

$$P_{\vec{K}m}(\vec{k}) = \sum_{\vec{g}} |C_{\vec{K}m}(\vec{g}+\vec{k}-\vec{K})|^2, \tag{9}$$

where $C_{\vec{K}m}$ represents the Fourier coefficients of the eigenstate $|\vec{K}m\rangle$, and $\vec{g}$ is a subset of the reciprocal-space vectors of the SC. Additional details regarding the calculations of the effective band structures of HDRCs are given in the Supplemental Material [47,48].

III. RESULTS AND DISCUSSION

We compare the reported experimental x-ray-diffraction (XRD) patterns obtained for $ReH_{0.5}$ at 18 GPa [21] and $ReH_{0.39}$ at 65 GPa [26] with those obtained from our corresponding predicted HDRC systems in Figs. 1(a) and 1(b), respectively. Here, the $ReH_{0.375}$ system given in Fig. 1(b) represents the closest match to $ReH_{0.39}$ based on the hydrogen solubility at that pressure. Notably, the experimentally derived XRD pattern in Fig. 1(b) includes peaks associated with hcp Re, and the peaks derived from $ReH_{0.39}$ are labeled with red tick marks at the bottom. The calculated XRD patterns are observed to be generally in good agreement with the corresponding experimental results. Therefore, we can conclude that the adopted computational methods are reliable.

We investigated the hydrogen solubility for a variety of HDRC systems at different pressures as a function of atomic hydrogen concentration based on their energetic stability, which was evaluated according to their calculated formation enthalpies (ΔH) relative to the products of dissociation in the pressure range of 1 bar to 50 GPa. The results are presented in Fig. 2(a). Those structures with ΔH values lying on the convex hull are considered thermodynamically stable, and therefore synthesizable experimentally. These systems are denoted by the filled marker symbols in the figure. The crystal structures of the HDRC systems adopted for these calculations are listed in Table S1 and illustrated in Fig. S4 in Supplemental Material [49–51]. We note that none of the HDRC systems are stable under ambient pressure, indicating that hydrogen is insoluble in Re without external pressure. We note that thermodynamically stable HDRC systems with increasing hydrogen concentration can only be obtained with increasing pressure, and that systems that are thermodynamically stable at a given pressure continue to be stable in a nonsaturated state at higher pressures. Finally, the results indicate that a fully stoichiometric Re hydride (ReH) system becomes thermodynamically stable at a pressure of 35 GPa.

The evolution in the hydrogen solubility of the HDRC systems with increasing pressure is illustrated in Fig. 2(b). Here, each bin presents all those HDRC systems that are thermodynamically stable at the specified pressure, and the hydrogen solubility is denoted by the maximum hydrogen concentration observed at that pressure, whereas the other systems represent unsaturated Re-H solid solutions. The observed monotonic increase in hydrogen dissolution with increasing pressure agrees well with corresponding experimental results [21,27]. The extent of this agreement is further investigated in Fig. 2(c), which plots the hydrogen concentrations of the saturated HDRC systems obtained from Fig. 2(b) as a function of pressure, and provides corresponding experimental results. We note that the overall trend in the hydrogen solubility obtained from the calculations agrees well with the experimental results, except that the rate at which the solubility increases with increasing pressure is greater for the calculations than that observed for the experimental results. This can be attributed to the fact that hydrogen atoms must surmount an energy barrier when diffusing into the Re host lattice in actual experiments, and therefore require higher temperatures and longer hydrogenation times to reach a saturated

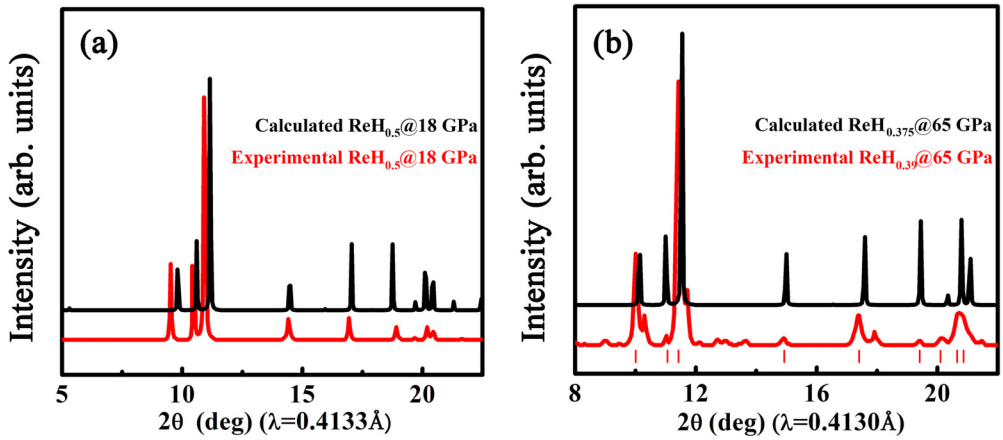

FIG. 1. Comparison of reported experimental XRD patterns and calculated XRD patterns for different HDRCs: (a) $ReH_{0.5}$ at 18 GPa; (b) $ReH_{0.39}$ (experimental) and $ReH_{0.375}$ (calculated) at 65 GPa. In (b), the experimental pattern includes peaks associated with the hcp phase of Re, and these peaks labeled with red tick marks at the bottom come from $ReH_{0.39}$.

state than under the conditions associated with the *ab initio* calculations [21].

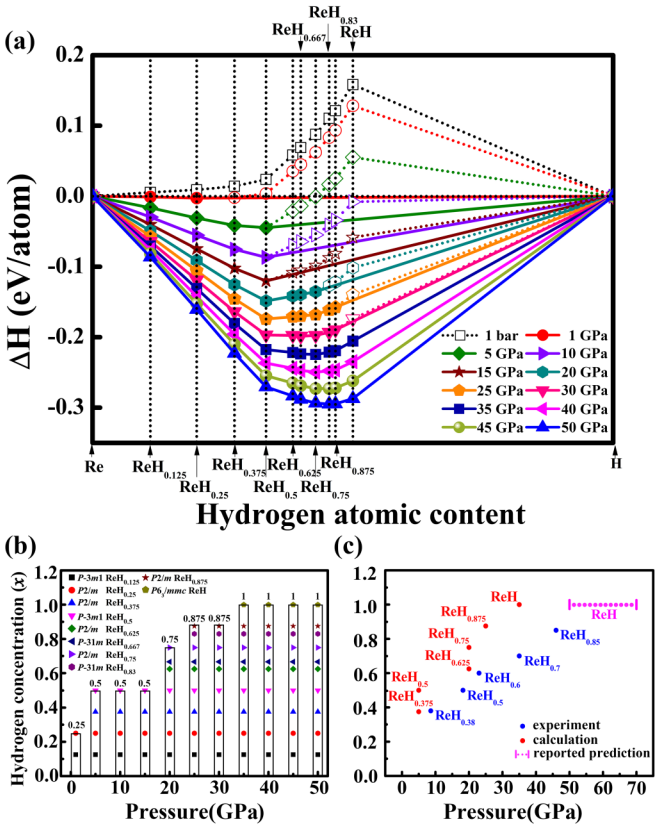

FIG. 2. (a) Calculated formation enthalpies (ΔH) of HDRCs as a function of atomic hydrogen concentration. The filled marker symbols represent thermodynamically stable HDRC systems at the corresponding pressures, and the open marker symbols represent metastable systems. (b) Evolution in the hydrogen solubility of solid HDRC solution systems with increasing pressure. (c) Relationship between HDRCs with saturated hydrogen concentrations and pressure obtained from (b) along with various experimentally derived values.

The thermodynamically stable HDRC structures predicted at a pressure of 50 GPa are illustrated in the inset of Fig. 3 and Fig. S2. In addition, the detailed atomic positions and lattice parameters of the predicted compounds are listed in Table S2 (Supplemental Material). The HDRCs can be described as interstitial hydrides, where, beginning with the hcp Re arrangement (Fig. S4), the HDRCs are obtained by filling the interstitial octahedral sites with hydrogen atoms. This is typified by the $ReH_{0.25}$ structure in which a hydrogen atom is captured within a Re cage, as shown in the inset of Fig. 3(b). In addition, the anti-CdI_2 type structure of $ReH_{0.5}$ and the NiAs-type structure of ReH are consistent with experimental results [21]. Comparison with the pure Re crystal structure (space group $P6_3/mmc$) indicates that the atomic configuration of the Re host lattice is basically preserved with increasing hydrogen concentration and pressure, except for shifts in the Re atom positions. For example, two Re atoms, denoted as Re1 and Re2, occupy the $2d$ position with a $-6m2$ site symmetry in the pure Re crystal, and the Re1 and Re2 positions are (0.333 33, 0.666 67, 0.750 00) and (0.666 66, 0.333 33, 0.250 00), respectively. However, the atoms Re1 and Re2 in the $ReH_{0.875}$ system move to positions (0.844 46, 0.171 70, 0.746 95) and (0.171 70, 0.844 46, 0.253 05), respectively, and the symmetry of the Re host lattice changes to that of the $P2/m$ space group. Accordingly, the Re1 to Re2 distance changes from 2.714 47 to 3.897 32 Å after hydrogen doping. The volumes of the HDRC systems increase with increasing hydrogen enrichment until the volume of the saturated ReH system is increased by 10.66% relative to that of the pure Re system.

The EBS calculations obtained for a series of HDRC systems are shown in Fig. 4 and Fig. S5 (Supplemental Material). The electronic energy band structure of the pure Re system is based on the $P6_3/mmc$ space group with a PC that is equivalent to a conventional cell [Fig. S5(a)]. The extent to which the Re host lattice is preserved in the HDRC systems can be evaluated by comparing the electronic band structure of pure Re with the unfolded electronic band structures obtained for the HDRC systems [Figs. 3(a)–3(d)] for $ReH_{0.125}$, $ReH_{0.5}$, $ReH_{0.875}$, and ReH, respectively, and Figs. S5(b) and S5(c) for $ReH_{0.375}$ and $ReH_{0.667}$, respectively). In contrast

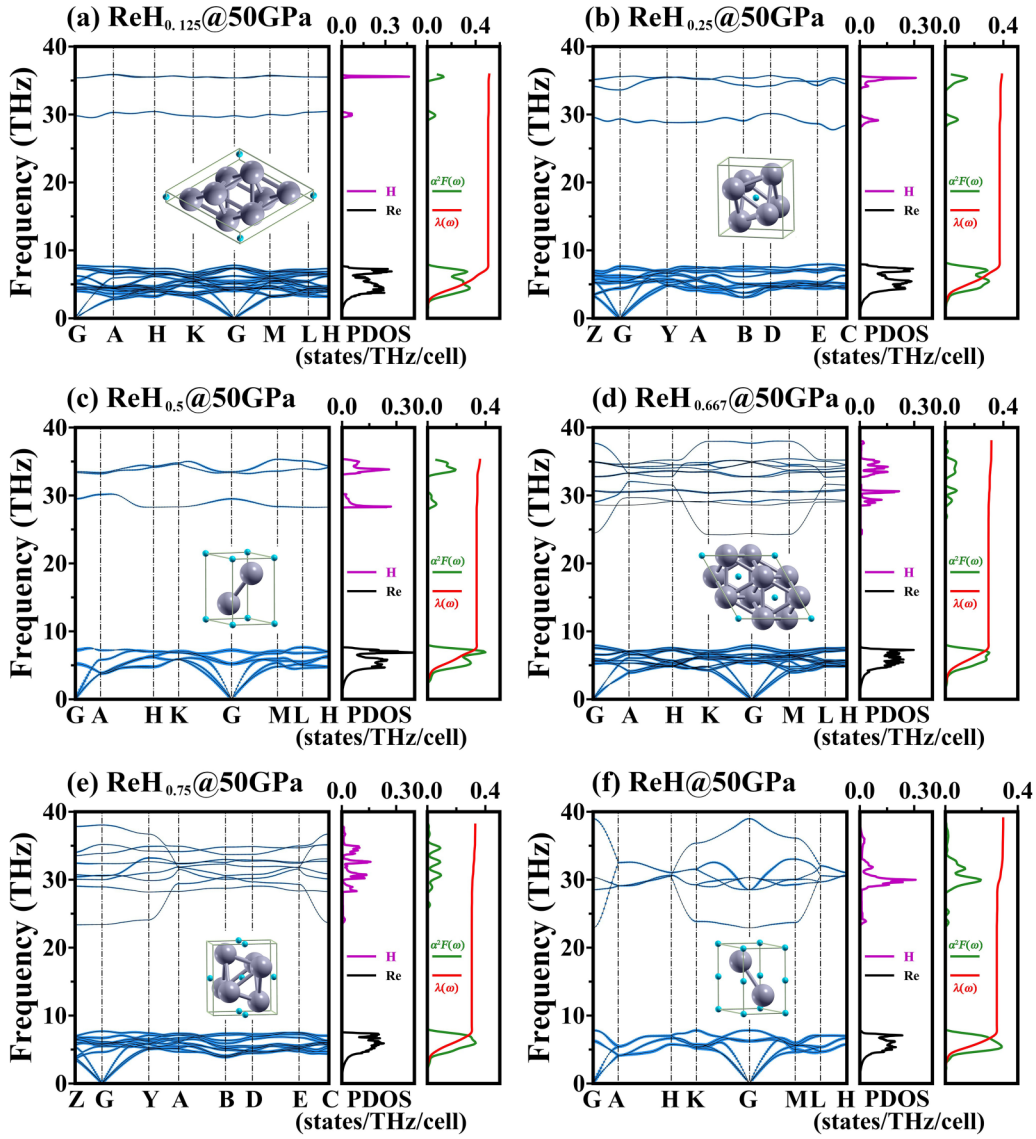

FIG. 3. Calculated lattice dynamics and superconductivity obtained for various HDRC systems at 50 GPa: (a) $ReH_{0.125}$ (space group $P\text{-}3m1$); (b) $ReH_{0.25}$ (space group $P2/m$); (c) $ReH_{0.5}$ (space group $P\text{-}3m1$); (d) $ReH_{0.667}$ (space group $P\text{-}3m1$); (e) $ReH_{0.75}$ (space group $P2/m$); (f) ReH (space group $P6_3/mmc$). The diagrams present phonon spectra, phonon density of states, Eliashberg phonon spectral function $\alpha^2F(\omega)$. The blue circles forming the bands represent the mode-resolved values of λ ($\lambda_{\mathbf{q}\upsilon}$), and the EPC strength increases with increasing circle diameter. The insets present the structures of the corresponding HDRC systems. The bonds given between Re atoms explicitly represent the bond structure of the pure Re host lattice.

to the unfolded electronic band structures obtained for the $ReH_{0.5}$ and ReH systems, we note that those obtained for the $ReH_{0.125}$, $ReH_{0.375}$, $ReH_{0.667}$, and $ReH_{0.875}$ systems present numerous broken and faint energy band lines originating from the occurrence of symmetry breaking. Although the atomic distributions in the SC appear to be ideal, the configurations of H atoms with different periods from Re atoms break the translational symmetry of the PC, and result in deviations from the Re host lattice [52]. However, the positions of the H atoms in the $ReH_{0.5}$ and ReH systems maintain consistent translational-symmetry configurations with respect to the Re host lattice. This implies that the H atoms in the $ReH_{0.5}$ and ReH systems should not be regarded as impurities, but as integral components in the crystal structures. Meanwhile, an increasing H concentration decreases the energy of the valence bands in the vicinity of the Fermi level, and thus decreases the electronic density of states at the Fermi level.

The dynamic stabilities of the HDRC systems at a pressure of 50 GPa can be further evaluated according to the phonon spectra and phonon density of states, respectively, shown in the left and middle panels of Fig. 3. No imaginary phonon frequencies can be observed across the entire Brillouin zone. Therefore, we can conclude that these structures are dynamically stable. Obviously, the higher-frequency modes in the range of $20-40$ THz mainly correspond to the vibration of H atoms owing to their lower mass, while the lower-energy modes correspond to the much more massive Re atoms.

A series of ReH_x compounds can be formed at 50 GPa, thus helping in investigating the effects of hydrogen enrichment on the superconductivity. The Eliashberg spectral function

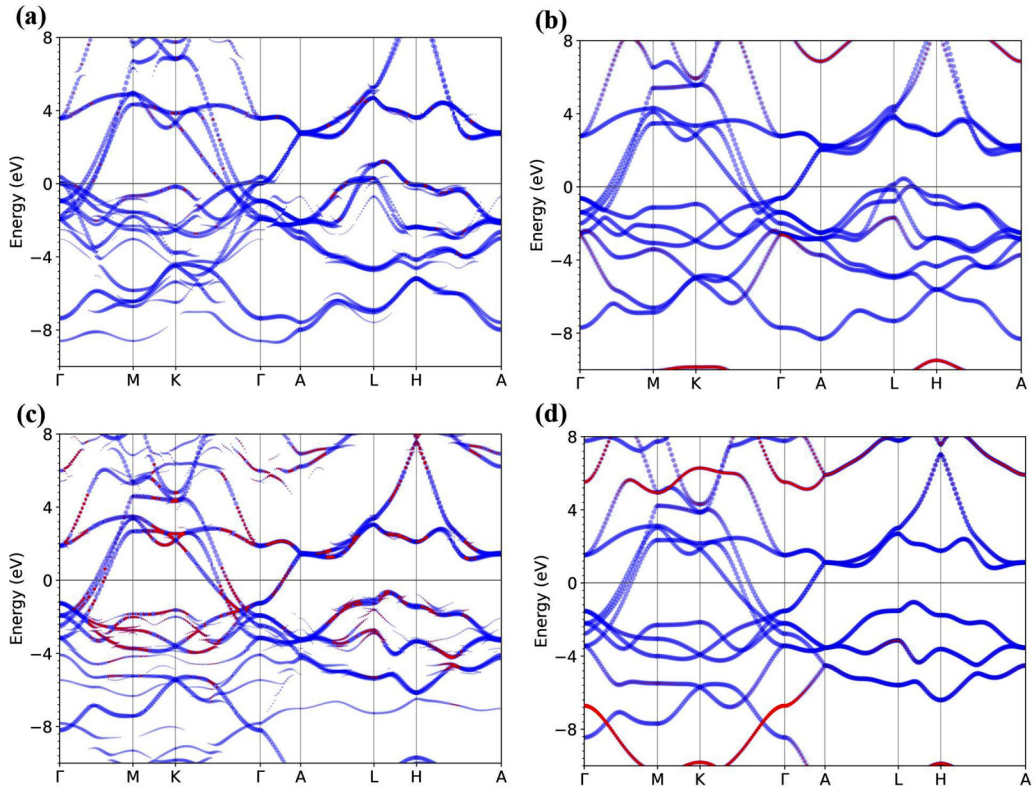

FIG. 4. Unfolded electronic band structures obtained for different HDRC systems at 50 GPa: (a) $ReH_{0.125}$; (b) $ReH_{0.5}$; (c) $ReH_{0.875}$; (d) ReH. The vertical lines represent high-symmetry points of the Brillouin zones. The blue and red circles forming the bands represent contributions from Re and H atoms, respectively, and the diameters of the circles increase as the proportions of the contributions obtained from the two species of atoms increase.

$\alpha^2F(\omega)$ and electron-phonon integral $\lambda(\omega)$ are presented in the right panels of Fig. 3. The EPC strength was projected on each vibration mode, and the magnitude of the EPC strength is represented in the figures based on the diameters of the blue circles forming the individual bands. The results clearly indicate that the values of λ are dominated by the phonon modes of the Re atoms. The calculated values of λ and $\omega_{\log}$ were employed to determine the corresponding values of T_c using Eq. (1) with a Coulomb pseudopotential value of $\mu^* = 0.1$ and 0.13. The calculated values of $N(\varepsilon_F)$, $\omega_{\log}$, λ, and T_c obtained for different HDRC systems at 50 GPa are listed in Table I. Here, $N(\varepsilon_F)$ was normalized to a formula unit that contains a single Re atom for comparison. The obtained values of T_c exhibit a decreasing trend with increasing hydrogen concentration up to the $ReH_{0.667}$ system, and then increase slightly with further increases in the hydrogen concentration, while an increasing hydrogen concentration promotes the high-frequency phonon modes and increases the values of $\omega_{\log}$, which play a positive role in enhancing T_c. An examination of Eq. (1) indicates that the decreasing trend in T_c with increasing hydrogen concentration is mainly attributable to the decreasing values of λ.

The rigid muffin-tin theory of Gaspari and Gyorffy [53] was applied for conducting further analysis of the

TABLE I. Calculated electronic density of states at the Fermi level $N(\varepsilon_F)$ (states/spin/Ry/f.u.), average logarithmic phonon frequency $\omega_{\log}$ (K), electron-phonon coupling parameter λ, superconducting critical temperature T_c (K), average electron-phonon matrix element $\langle I^2\rangle/M$ [eV · (THz)^2], and average phonon frequency $\langle\omega^2\rangle^{1/2}$ (THz), obtained for different HDRC systems at 50 GPa. The values of $N(\varepsilon_F)$ have been normalized to a formula unit that contains a single Re atom for comparison.

System (space group)	$N(\varepsilon_F)$	$\omega_{\log}$	$\langle\omega^2\rangle^{1/2}$	λ	T_c (K)	$\langle I^2\rangle/M$
Re ($P6_3/mmc$)	5.09	227	31.58	0.575	3.10–4.54	766
$ReH_{0.125}$ (P-3m1)	4.57	244	42.02	0.519	2.14–3.41	341
$ReH_{0.25}$ ($P2/m$)	4.00	282	54.17	0.396	0.48–1.12	988
$ReH_{0.5}$ (P-3m1)	3.60	314	64.05	0.356	0.20–0.62	2762
$ReH_{0.667}$ (P-3m1)	3.36	316	64.72	0.319	0.05–0.27	900
$ReH_{0.75}$ ($P2/m$)	3.30	320	65.36	0.329	0.09–0.35	1451
ReH ($P6_3/mmc$)	3.22	319	72.42	0.324	0.07–0.31	3592

observed variation in the values of λ obtained for the various HDRC systems. For this purpose, the following simplified expression for λ in the McMillan-Hopfield form was adopted:

$$\lambda = \frac{\eta}{M\langle\omega^2\rangle} = \frac{N(\varepsilon_F)\langle I^2\rangle}{M\langle\omega^2\rangle}, \tag{10}$$

where M is the atomic mass, $\langle I^2\rangle$ is the average electron-phonon matrix element over the Fermi surface, and $\langle\omega^2\rangle$ is the average squared phonon frequency, which is given as follows:

$$\langle\omega^2\rangle = \frac{2}{\lambda}\int_0^\infty \omega\alpha^2F(\omega)d\omega. \tag{11}$$

The calculated values of $\langle I^2\rangle/M$ and $\langle\omega^2\rangle^{1/2}$ obtained for different HDRC systems at 50 GPa are listed in Table I. The results in Table I indicate that $N(\varepsilon_F)$ decreases and $\langle\omega^2\rangle$ increases monotonically with increasing hydrogen concentration. According to Eq. (10), these contrary trends are the dominant features responsible for the decreasing λ observed with increasing hydrogen concentration. Moreover, we note that the minimum value of λ obtained for the $ReH_{0.667}$ system can be attributed to the sudden decrease in $\langle I^2\rangle/M$ observed at that hydrogen concentration.

Considering the dominant roles of $\langle\omega^2\rangle$ and $N(\varepsilon_F)$ in determining the trend in the value of λ observed for the HDRC systems, the effects of hydrogen concentration on λ can be further analyzed by evaluating the phonon frequencies and electronic properties of the systems. As shown in Fig. 3 and Fig. S6(f), hydrogen dissolution leads to higher phonon frequencies in H-doped compounds as compared to those of pure Re. The vibration frequencies in HDRC systems demonstrate an escalating trend with increasing hydrogen enrichment. It is easy to understand that the hardening phonon frequencies originate from the light atomic mass of hydrogen. We note from Table I that the value of $\langle\omega^2\rangle^{1/2}$ obtained for the ReH system is more than twice the value obtained for the pure Re system at the same pressure. Moreover, the optical modes of hydrogen broaden (i.e., the phonon bandwidth increase), particularly for systems with hydrogen concentrations greater than 0.5 owing to the progressively decreasing distance between adjacent H atoms in the Re-H solid solutions (Table S4). However, it is worth noting here that neither H2 nor H3 units were formed as observed in previously reported hydrides [54,55]. While the effect of hydrogen atoms on increasing the phonon frequencies of hydrides is widely reported, a large difference still exists in the phonon dispersion characteristics of high-T_c superconductive hydrogen-rich compounds and HDRCs. Here, the optical modes possess the nature of distributing with a broad energy range or strongly depend on the wave vectors [56–59]. This in turn enhances the probability of satisfying the formation energy of Cooper pairs and would be beneficial to strong EPC [58]. As for the HDRC systems in this study, similar features are absent in the optical phonon branches. The very weak H–H bonds in these interstitial hydrides decrease the overall level of electron-phonon interaction, and thus produce a very small electron-phonon matrix element, which leads to the low-T_c features of the HDRC systems relative to the high-T_c features in H-rich hydrides.

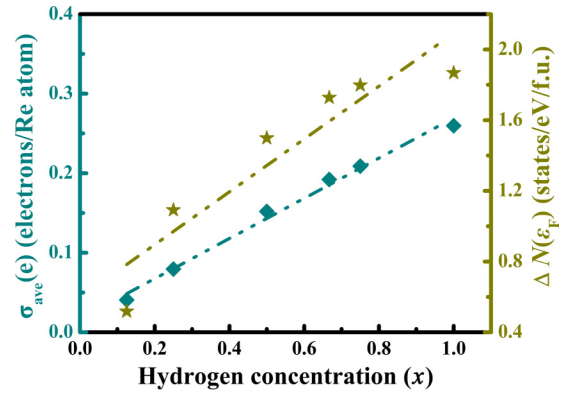

FIG. 5. Evolution of σ_{ave} and $\Delta N(\varepsilon_F)$ with increasing hydrogen concentration at a pressure of 50 GPa, where σ_{ave} represents the average number of donated electrons per Re atom and $\Delta N(\varepsilon_F)$ represents the difference between the normalized value of $N(\varepsilon_F)$ obtained for the pure Re system and a given HDRC system. The dotted lines were obtained by fitting to the data using the least-squares method.

The decreasing trend observed for the $N(\varepsilon_F)$ values of the HDRC systems with increasing hydrogen concentration (Table I) can be roughly evaluated from the perspective of the results of Bader charge analysis [60] (Table S3) and the projected electronic density of states (PDOS) (Fig. S7) obtained for the various systems. The Bader charge analysis results indicate that H atoms function as hole donors, and the number of electrons donated from per Re to the H atoms increases with increasing H concentration (Table S3). Notably, the difference of $N(\varepsilon_F)$ between pure Re and the HDRC systems exhibits a continuous increase along with an increasing hydrogen concentration (see Fig. 5). According to the PDOS, the Re atoms are primarily responsible for the values of $N(\varepsilon_F)$ obtained for the HDRC systems. Therefore, the increasing donation of electrons by Re atoms under increasing hydrogen dissolution leads to the declining of $N(\varepsilon_F)$ and the subsequent EPC λ. So, the increasing H solubility pulls down the EPC λ and T_c in the HDRC.

Moreover, the effects of pressure on the superconductivity of the HDRC systems were also investigated. To this end, the values of λ and T_c were calculated for the pure Re and $ReH_{0.5}$ systems at different pressures (Tables S5 and S6) based on the results of the corresponding phonon spectra, phonon density of states, and $\alpha^2F(\omega)$ spectra (Figs. S6 and Fig. S8). The results indicate that the values of T_c obtained for both the Re and $ReH_{0.5}$ systems decrease monotonically with increasing pressure, and that this trend is dominated by a decreasing value of λ. Similar to the role of increasing H concentration in Re-H systems at a pressure of 50 GPa, an increasing pressure is observed to result in an increasing value of $\langle\omega^2\rangle$ and a decreasing value of $N(\varepsilon_F)$ in both the pure Re and $ReH_{0.5}$ systems, resulting in decreasing values of λ and T_c.

Accordingly, the occurrence of superconductivity in the Re-H systems is regulated not only by the pressure, but also by an increasing hydrogen concentration, which itself increases with increasing pressure. Therefore, the superconductivity mechanism of the HDRC systems was explored by comparing

the superconductivity observed in the pure Re system (Table S5 and Fig. S6) and HDRC systems under varying pressure. The values of $N(\varepsilon_F)$, $\omega_{\log}$, λ, T_c, $\langle I^2\rangle/M$, and $\langle\omega^2\rangle^{1/2}$ of saturated hydrogen solid solutions of $ReH_{0.5}$, $ReH_{0.75}$, and ReH obtained at pressures of 5 GPa, 20 GPa, and 35 GPa, respectively, were calculated (Table S7) based on the results of the corresponding phonon spectra, phonon density of states, and $\alpha^2F(\omega)$ spectra (Fig. S9). As expected, T_c exhibits a decreasing trend from 0.64–1.36 K to 0.15–0.49 K over the full range of increasing hydrogen concentration and pressure. This is again mainly attributable to a decreasing value of λ, which is again observed to arise owing to an increasing $\langle\omega^2\rangle^{1/2}$ and a descending $N(\varepsilon_F)$. Here, we note that the value of $\langle\omega^2\rangle^{1/2}$ obtained for the pure Re increased by 18.7% with increasing pressure from 5 to 35 GPa (Table S5). Meanwhile, considering both increasing pressure and increasing hydrogen concentration according to the solubility obtained at that pressure (Table S7), we find that the value of $\langle\omega^2\rangle^{1/2}$ obtained for the corresponding HDRC systems increased by 32.7% over the same pressure range. These results clearly demonstrate the direct effects of both pressure and hydrogen concentration on $\langle\omega^2\rangle^{1/2}$. Similarly, the value of $N(\varepsilon_F)$ obtained for the pure Re system decreases with increasing pressure from 5 to 35 GPa by 7.7% (Table S5), while this value increases by 14.6% over the same pressure range for the saturated HDRC systems (Table S7). Moreover, the values of $N(\varepsilon_F)$ obtained for the saturated HDRC systems at a given pressure are considerably less than those obtained for the pure Re system at the same pressure, and the values of $\Delta N(\varepsilon_F)$ generally increase with increasing pressure owing to the increasing value of x obtainable at higher pressures. As discussed previously, this can ultimately be attributed to the increasing charge donation of the Re atoms with increasing hydrogen concentration (Tables S5, S8, and S9, and Fig. S10). In this sense, H doping exerts a similar effect as the pressure on the superconductivity of solid solution Re-H compounds.

IV. CONCLUSION

The dissolution of hydrogen in Re, and the electronic properties, lattice dynamics, and EPC in the corresponding interstitial Re hydrides have been investigated systematically by means of *ab initio* calculations. A series of thermodynamically stable ReH_x systems were predicted over a wide range of external pressures from 1 bar to 50 GPa. The mutual effects of hydrogen concentration and pressure on the EPC of doped compounds were analyzed by comparing the hydrogen concentration and pressure dependences of the EPC parameter λ obtained for pure Re and HDRC systems. The decreasing trend in λ observed for the ReH_x systems under increasing x was demonstrated to be dominated by a corresponding increase in the average squared phonon frequencies $\langle\omega^2\rangle$ and decrease in the electronic density of states $N(\varepsilon_F)$ at the Fermi level. These trends in turn were demonstrated to follow, respectively, from the increasing concentration of low-mass H atoms and an increasing donation of electrons by Re atoms under increasing hydrogen dissolution.

ACKNOWLEDGMENTS

This work was supported by the National Key R&D Program of China (Grant No. 2018YFA0305900), National Natural Science Foundation of China (Grants No. 11774119, No. 11904187, No. 51632002, No. 51572108, No. 91745203, No. 11634004, and No. 11174102), National Key Research and Development Program of China (Grant No. 2016YFB0201204), Program for Changjiang Scholars and Innovative Research Team in University (Grant No. IRT_-15R23), National Fund for Fostering Talents of basic Science (Grant No. J1103202), and Doctoral Scientific Research Foundation of Inner Mongolia University for Nationalities (Grant No. BS480). Parts of calculations were performed in the High Performance Computing Center (HPCC) of Jilin University.

[1] Y. Ma, M. Eremets, A. R. Oganov, Y. Xie, I. Trojan, S. Medvedev, A. O. Lyakhov, M. Valle, and V. Prakapenka, Nature (London) **458**, 182 (2009).

[2] X. Dong, A. R. Oganov, A. F. Goncharov, E. Stavrou, S. Lobanov, G. Saleh, G. Qian, Q. Zhu, C. Gatti, V. L. Deringer, R. Dronskowski, X. Zhou, V. Prakapenka, Z. Konôpková, I. Popov, A. I. Boldyrev, and H. Wang, Nat. Chem. **9**, 440 (2017).

[3] A. P. Drozdov, M. I. Eremets, I. A. Troyan, V. Ksenofontov, and S. I. Shylin, Nature (London) **525**, 73 (2015).

[4] A. P. Drozdov, P. P. Kong, V. S. Minkov, S. P. Besedin, M. A. Kuzovnikov, S. Mozaffari, L. Balicas, F. Balakirev, D. Graf, V. B. Prakapenka, E. Greenberg, D. A. Knyazev, M. Tkacz, and M. I. Eremets, Nature (London) **569**, 528 (2019).

[5] M. Somayazulu, M. Ahart, A. K Mishra, Z. M. Geballe, M. Baldini, Y. Meng, V. V. Struzhkin, and R. J. Hemley, Phys. Rev. Lett. **122**, 027001 (2019).

[6] E. Snider, N. Dasenbrock-Gammon, R. McBride, M. Debessai, H. Vindana, K. Vencatasamy, K. V. Lawler, A. Salamat, and R. P. Dias, Nature (London) **586**, 373 (2020).

[7] X. Jin, X. Chen, T. Cui, H. Mao, H. Zhang, Q. Zhuang, K. Bao, D. Zhou, B. Liu, Q. Zhou, and Z. He, Proc. Natl. Acad. Sci. USA **113**, 2366 (2016).

[8] W. Zhang, A. R. Oganov, A. F. Goncharov, Q. Zhu, S. E. Boulfelfe, A. O. Lyakhov, E. Stavrou, M. Somayazulu, V. B. Prakapenka, and Z. Konôpková, Science **342**, 1502 (2013).

[9] L. Chen, P. Chen, W. Li, Q. Zhang, V. V. Struzhkin, A. F. Goncharov, Z. Ren, and X. Chen, Nat. Mater. **18**, 1321 (2019).

[10] N. W. Ashcroft, Phys. Rev. Lett. **21**, 1748 (1968).

[11] Q. Zhuang, X. Jin, T. Cui, D. Zhang, Y. Li, H. Yu, K. Bao, and B. Liu, Phys. Lett. A **384**, 126571 (2020).

[12] R. P. Dias and I. F. Silvera, Science **355**, 715 (2017).

[13] B. Zhang, S. Ma, I. Rachmin, M. He, P. Baral, S. Choi, W. A. Gonçalves, Y. Shwartz, E. M. Fast, Y. Su, L. I. Zon, A. Regev, J. D. Buenrostro, T. M. Cunha, I. M. Chiu, D. E. Fisher, and Y. Hsu, Nature (London) **577**, 676 (2020).

[14] N. W. Ashcroft, Phys. Rev. Lett. **92**, 187002 (2004).

[15] X. Jin, X. Meng, Z. He, Y. Ma, B. Liu, T. Cui, G. Zou, and H. Mao, Proc. Natl. Acad. Sci. USA **107**, 9969 (2010).

[16] Q. Zhuang, X. Jin, T. Cui, Y. Ma, Q. Lv, Y. Li, H. Zhang, X. Meng, and K. Bao, Inorg. Chem. **56**, 3901 (2017).

[17] M. I. Eremets, I. A. Trojan, S. A. Medvedev, J. S. Tse, and Y. Yao, Science **319**, 1506 (2008).

[18] P. Loubeyre, F. Occelli, and P. Dumas, Nature (London) **577**, 631 (2020).

[19] H. Liu, I. I. Naumov, R. Hoffmann, N. W. Ashcroft, and R. J. Hemley, Proc. Natl. Acad. Sci. USA **114**, 6990 (2017).

[20] H.-K. Mao, X.-J. Chen, Y. Ding, B. Li, and L. Wang, Rev. Mod. Phys. **90**, 015007 (2018).

[21] T. Scheler, O. Degtyareva, and E. Gregoryanz, J. Chem. Phys. **135**, 214501 (2011).

[22] P. Loubeyre, F. Occelli, and R. LeToullec, Nature (London) **416**, 613 (2002).

[23] P. Dalladay-Simpson, R. T. Howie, and E. Gregoryanz, Nature (London) **529**, 63 (2016).

[24] T. Scheler, M Marqués, Z Konôpková, C. L. Guillaume, R. T. Howie, and E. Gregoryanz, Phys. Rev. Lett. **111**, 215503 (2013).

[25] N. P. Salke, M. M. D. Esfahani, Y. Zhang, I. A. Kruglov, J. Zhou, Y. Wang, E. Greenberg, V. B. Prakapenka, J. Liu, A. R. Oganov, and J.-F. Lin, Nat. Commun. **10**, 4453 (2019).

[26] O. Degtyareva, J. E. Proctor, C. Guillaume, E. Gregoryanz, and M. Hanfland, Solid State Commun. **149**, 1583 (2009).

[27] T. Atou and J. V. Badding, J. Solid State Chem. **118**, 299 (1995).

[28] S. P. Besedin and A. P. Jephcoat, Rev. High Pressure Sci. Technol. **7**, 301 (1998).

[29] H. Kawamura, M. Harada, Y. Akahama, and K. Takemura, Solid State Commun. **130**, 59 (2004).

[30] V. E. Antonov, I. T. Belash, O. V. Zharikov, and A. V. Palnichenko, Phys. Status Solidi B **142**, K155 (1987).

[31] Y. Li, X. Jin, T. Cui, Q. Zhuang, Q. Lv, G. Wu, X. Meng, K. Bao, B. Liu, and Q. Zhou, RSC Adv. **7**, 7424 (2017).

[32] Q. Zhuang, X. Jin, Q. Lv, Y. Li, Z. Shao, Z. Liu, X. Li, H. Zhang, X. Meng, K. Bao, and T. Cui, Phys. Chem. Chem. Phys. **19**, 26280 (2017).

[33] D. Zhang, X. Jin, Q. Zhuang, Y. Li, S. Yang, L. Song, B. Liu, and T. Cui, Chin. Phys. B **28**, 056101 (2019).

[34] H. Zhang, X. Jin, Y. Lv, Q. Zhuang, Y. Liu, Q. Lv, D. Li, K. Bao, B. Liu, and T. Cui, RSC Adv. **5**, 107637 (2015).

[35] Q. Zhuang, X. Jin, K. Bao, and T. Cui, New J. Phys. **22**, 033011 (2020).

[36] Y. Li, X. Jin, T. Cui, Q. Zhuang, D. Zhang, X. Meng, K. Bao, B. Liu, and Q. Zhou, RSC Adv. **7**, 44884 (2017).

[37] A. R. Oganov and C. W. Glass, J. Chem. Phys. **124**, 244704 (2006).

[38] G. Kresse and J. Furthmüller, Phys. Rev. B **54**, 11169 (1996).

[39] J. P. Perdew, K. Burke, and M. Ernzerhof, Phys. Rev. Lett. **77**, 3865 (1996).

[40] P. Giannozzi, S. Baroni, N. Bonini, M. Calandra, R. Car, C. Cavazzoni, D. Ceresoli, G. L. Chiarotti, M. Cococcioni, I. Dabo, A. Dal Corso, S. de Gironcoli, S. Fabris, G. Fratesi, R. Gebauer, U. Gerstmann, C. Gougoussis, A. Kokalj, M. Lazzeri, L. Martin-Samos, N. Marzari, F. Mauri, R. Mazzarello, S. Paolini, A. Pasquarello, L. Paulatto, C. Sbraccia, S. Scandolo, G. Sclauzero, A. P. Seitsonen, A. Smogunov, P. Umari, and R. M. Wentzcovitch, J. Phys.: Condens. Matter **21**, 395502 (2009).

[41] The pseudopotentials of Re and H are downloaded from the official website of QUANTUM-ESPRESSO code, http://www.quantum-espresso.org/pseudopotentials.

[42] S. Baroni, S. de Gironcoli, A. Dal Corso, and P. Giannozzi, Rev. Mod. Phys. **73**, 515 (2001).

[43] P. B. Allen and R. C. Dynes, Phys. Rev. B **12**, 905 (1975).

[44] V. Popescu and A. Zunger, Phys. Rev. Lett. **104**, 236403 (2010).

[45] W. Ku, T. Berlijn, and C. C. Lee, Phys. Rev. Lett. **104**, 216401 (2010).

[46] V. Popescu and A. Zunger, Phys. Rev. B **85**, 085201 (2012).

[47] See Supplemental Material at http://link.aps.org/supplemental/10.1103/PhysRevB.103.174520 for the details of the ELOCR code and effective band structures, the depictions of crystal structures, electronic properties, phonon dispersions, electron-phonon coupling features for pure Re and the interstitial hydrides.

[48] https://www.vasp.at/wiki/index.php/WAVECAR, and http://www.andrew.cmu.edu/user/feenstra/wavetrans.

[49] L. Cui, N. H. Chen, and I. F. Silvera, Phys. Rev. B **51**, 14987 (1995).

[50] P. Loubeyre, R. Letoullec, D. Hausermann, M. Hanfland, R. J. Hemley, H. K. Mao, and L. W. Finger, Nature (London) **383**, 702 (1996).

[51] C. J. Pickard and R. J. Needs, Nat. Phys. **3**, 473 (2007).

[52] Y. Ikeda, A. Carreras, A. Seko, A. Togo, and I. Tanaka, Phys. Rev. B **95**, 024305 (2017).

[53] G. D. Gaspari and B. L. Gyorffy, Phys. Rev. Lett. **28**, 801 (1972).

[54] Y. Cheng, C. Zhang, T. Wang, G. Zhong, C. Yang, X. Chen, and H. Lin, Sci. Rep. **5**, 16475 (2015).

[55] X. Zhong, H. Wang, J. Zhang, H. Liu, S. Zhang, H.-F. Song, G. Yang, L. Zhang, and Y. Ma, Phys. Rev. Lett. **116**, 057002 (2016).

[56] K. Tanaka, J. S. Tse, and H. Liu, Phys. Rev. B **96**, 100502(R) (2017).

[57] H. Wang, J. S. Tse, K. Tanaka, T. Iitaka, and Y. Ma, Proc. Natl. Acad. Sci. USA **109**, 6463 (2012).

[58] Q. Zhuang, X. Jin, T. Cui, D. Zhang, Y. Li, X. Li, K. Bao, and B. Liu, Phys. Rev. B **98**, 024514 (2018).

[59] F. Peng, Y. Sun, C. J. Pickard, R. J. Needs, Q. Wu, and Y. Ma, Phys. Rev. Lett. **119**, 107001 (2017).

[60] R. F. W. Bader, Acc. Chem. Res. **18**, 9 (1985).